Aerial Measurement of Radiation Temperatures over Mt. Fuji and Tokyo Areas and Their Application to the Determination of Ground- and Water-Surface Temperatures

TETSUYA FUJITA, GISELA BARALT, AND KIYOSHI TSUCHIYA

Reprinted from JOURNAL OF APPLIED METEOROLOGY, Vol. 7, No. 5, pp. 801–816, October 1968

Reprinted from JOURNAL OF APPLIED METEOROLOGY, Vol. 7, No. 5, October 1968, pp. 801–816
American Meteorological Society
Printed in U. S. A.

Aerial Measurement of Radiation Temperatures over Mt. Fuji and Tokyo Areas and Their Application to the Determination of Ground- and Water-Surface Temperatures[1]

TETSUYA FUJITA AND GISELA BARALT

The University of Chicago

AND KIYOSHI TSUCHIYA

Japan Meteorological Agency, Tokyo

(Manuscript received 10 April 1968)

ABSTRACT

A Barnes PRT-4 portable radiometer with a spectral response in the 8–14 μ range was used to determine the equivalent blackbody temperature of 1) the slope of Mt. Fuji, 2) Sagami Bay, and 3) the city of Tokyo. A twin-engine aircraft was used to fly over these areas at various altitudes up to 12,000 ft. Through mapping the slope temperatures of Mt. Fuji, it was learned that the rocky slope heats up under the morning sun very rapidly to 32C almost irrespective of the elevation. The distribution of measured temperatures explains the reasons for the rapid growth of cumulus clouds along the east slope in the early morning hours. The nadir angle and the height dependence of equivalent blackbody temperatures measured over Tokyo and Sagami Bay were examined. The measured temperatures were compared with those computed from the radiative transfer equation. It was found that the values over Tokyo are reproduced fairly well by the addition of a graybody smog filling the layers up to 910 mb. To express the effects of atmospheric radiation upon the reduction of the radiant emittance from the surface, a damping factor was introduced. The factor which designates the reduction of the amplitude of the surface temperature when measured from aircraft or satellites must be known to an accuracy of about 10% in order to estimate the true temperature variation or gradient from measured equivalent blackbody temperatures. Further investigation of the temperature damping is necessary to determine accurately the radiometric sea-surface temperature.

1. Introduction

As a result of the latest development in infrared radiometers which can be operated on board an aircraft or a satellite, their applications to meteorology are increasing rapidly. Combs *et al.* (1965) made aerial measurements of ground and cloud temperatures by using Barnes R-4D1 industrial radiometers with a spectral response extending from 8 to beyond 32 μ and a model 14-310 radiometer with 8–13 μ spectral response. Their study showed that the emissivity of various types of soil exceeds 0.96 except for beach sand, making it possible to assume blackbody radiation at the surface for most practical purposes. The equivalent blackbody temperatures measured from an aircraft flying over Arizona showed a significant contribution from the atmosphere located beneath the flight level. An 18.5C reduction of the desert temperature was obtained when measured from 10,500 ft and the reduction was only 4.6C when the radiometer was pointed toward the adjacent irrigated field. The atmosphere over the desert and the adjacent field may be regarded identical in terms of vertical distribution of temperature and moisture. In other words, the temperature difference of 26.2C between the desert (60.2C) and the field (34.0C) was reduced to only 12.3C when measured from the 10,500-ft level.

Effects of atmospheric radiation in airborne measurements of surface temperature were estimated by Lenschow and Dutton (1964). Since their main concern was to measure surface temperatures from a low-flying airplane equipped with a radiometer of a 20° field of view, the measured radiation was separated into the energy from the ground and that from the atmosphere assumed to be of a uniform temperature. Then they obtained an equation for computing the surface temperature from the measured temperature, air temperature, and a parameter indicating the ratio of the increments in measured and air temperatures. Recent measurements by Kuhn and McFadden (1967) revealed the importance of atmospheric radiation in determining surface temperatures by airborne radiometers.

Despite the fact that the atmosphere beneath the flight level attenuates the outgoing radiation from the underlying surface while reradiating at its temperature, resulting sometimes in a significant difference between measured and actual temperatures, a window-channel radiometer can be used for indirect measurements of

[1] The research reported in this paper has been sponsored by ESSA (MSL) under Grant Cwb WBG-34 and NASA under Grant NsG 333. The portion of the research performed in Japan was supported by US-Japan cooperative science program under Grants NSF GF-255 and JSPS GEO-19.

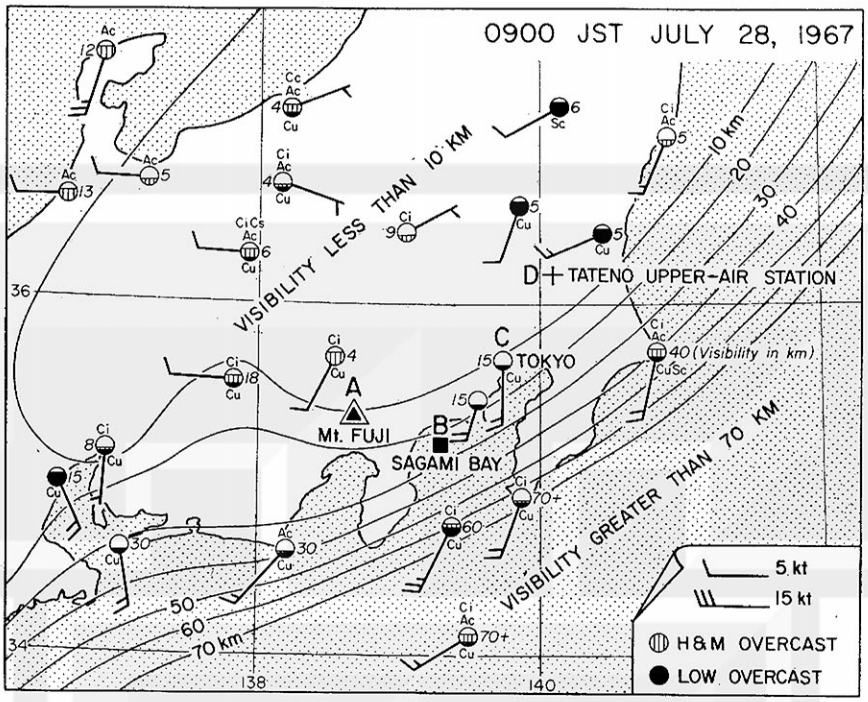

FIG. 1. Surface chart showing the distribution of clouds and visibility at 0900 JST 28 July 1967, the day of radiation measurements over Mt. Fuji, Sagami Bay and Tokyo.

ground- or water-surface temperature from the air. Aerial measurements of the sea surface by Lorenz (1966, 1967), for example, demonstrated the capability of detecting warm and cold spots as well as the thermal gradients on the sea surface.

Our radiation measurements over the Mt. Fuji and Tokyo areas were carried out by using a Barnes PRT-4 radiometer in an attempt to obtain the surface temperature of the city, the mountain, and a bay between them. Shown in Fig. 1 are the isolines of visibility contoured at 10-km intervals and the locations of Mt. Fuji, A; Sagami Bay, B; Tokyo, C; and the upper-air station at Tateno, D. The radiometric measurements were made from a twin-engine aircraft based at Haneda International Airport southwest of Tokyo. Five flights were made between 0400 and 1800 28 July 1967.

2. Spatial and spectral responses of PRT-4 radiometer

The Barnes PRT-4 is a portable radiometer with its output either read from an indicator dial or recorded with an Esterline Angus recorder. We took advantage of both capabilities so that any change in measured temperature could be noticed immediately while obtaining a continuous record for later data reduction and analyses.

The field of view at the half-power point is 2°, equivalent to the radiant emittance which would be received from a circular area 35 m in diameter when viewed straight down from 1000 m above the ground. The full-power field of view naturally extends much beyond the circle. Nevertheless, the hand-held operation permitted us to measure the radiation from relatively small areas such as bridges on rivers, playgrounds, railroad yards, etc.

The spectral response of the radiometer extends between 7.4 and 16.0 μ with an insignificant response near 19 μ. Presented in Fig. 2 is the distribution of the spectral response ϕ_λ, excluding that around 19 μ. The spectral radiant emittance of a blackbody, $B(\lambda,T)$ [W m^{-2} μ^{-1}] was computed at 10C intervals between -20 and 50C to determine the spectral radiant emittance $W(\lambda,T)$ filtered by the radiometer's optical system. Fig. 2 shows that the wavelength giving rise to the maximum contribution shifts from 9.5 toward 12 μ as the blackbody temperature decreases to -20C.

The effective radiant emittance as defined by NASA (1961) was then computed from

$$\bar{W}=\int_0^\infty B(\lambda,T)\phi_\lambda d\lambda, \qquad (1)$$

which denotes that portion of blackbody radiant emittance which would be detected by a sensor with a spectral response ϕ_λ when the field of view is completely filled with a unique temperature radiator. It should be noted that no atmospheric absorption is assumed to exist between the sensor and the blackbody radiator when $\bar{W}$ is computed as a function of temperature using Eq. (1). The results of such computations for the radiometer are shown in Fig. 3.

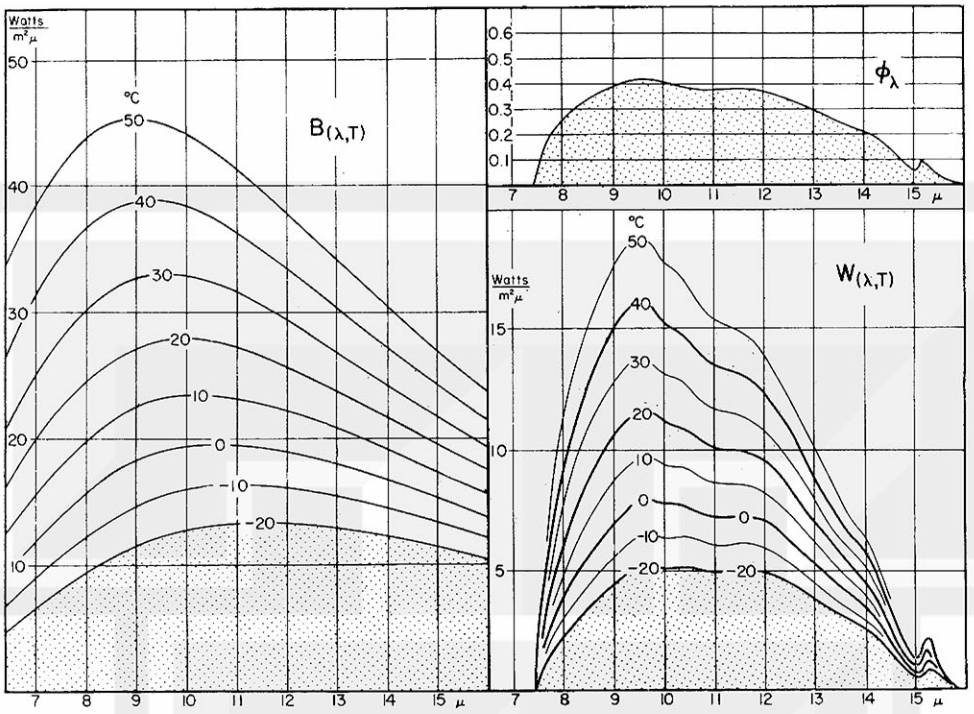

FIG. 2. The Planckian radiant emittance $B(\lambda,T)$ between -20 and 50C and the spectral radiant emittance $W(\lambda,T)$ over the same temperature range, obtained by multiplying by the spectral response ϕ_λ of a Barnes PRT-4 shown in the upper right diagram.

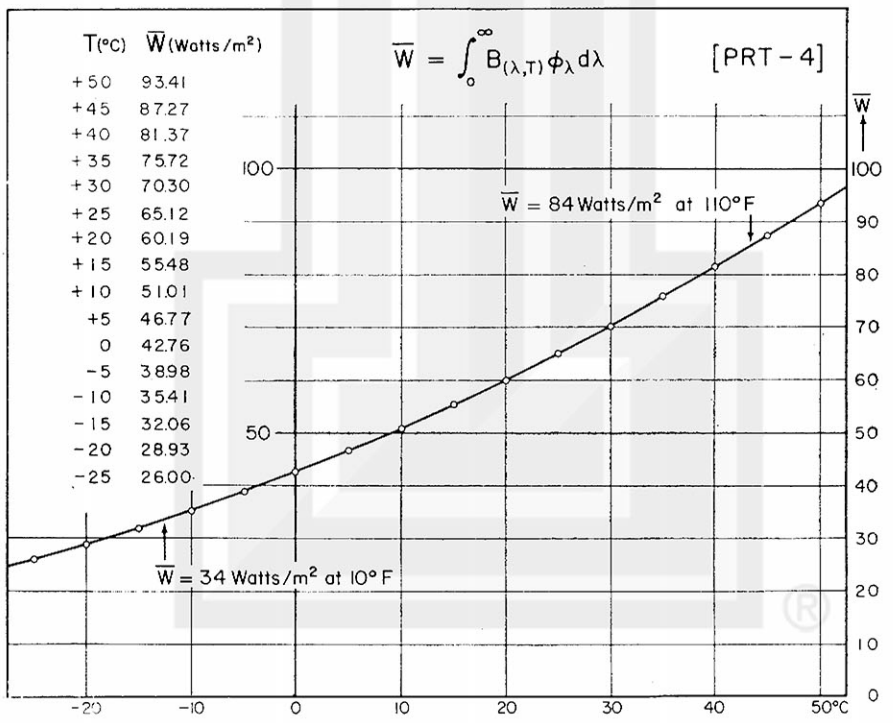

FIG. 3. The effective radiant emittance $\bar{W}$ of a Barnes PRT-4 radiometer. At about 40C the chopper temperature of the unit used in this experiment was so low that the output reading in mV showed a reversed response when the radiometer was calibrated on the ground by pointing it toward hot objects heated by the sun.

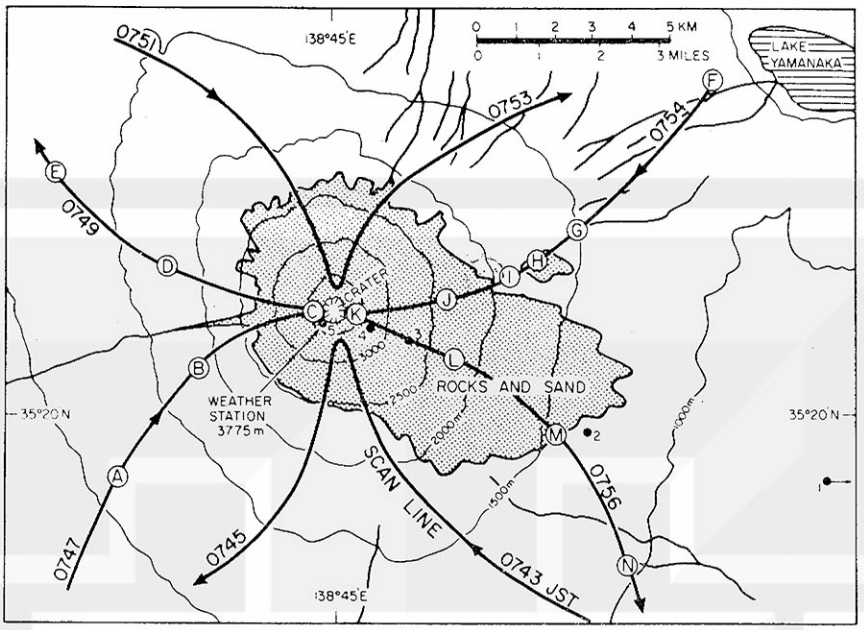

FIG. 4. Four scan lines on the slope of Mt. Fuji, a 3776-m (12,886 ft) volcano. These scans were made on 28 July 1967 from an aircraft at 12,000 ft while circling the peak keeping a radius of about 13 km. The stippled areas are the ground with loose rocks and sand mostly free from trees.

The radiation transfer equation as discussed by Greenfield and Kellogg (1960) can be written as

$$\bar{W}=\int\int \phi_\lambda B(\lambda,T)d\tau d\lambda+\int e_s\tau_{s\lambda}\phi_\lambda B(\lambda,T_s)d\lambda, \quad (2)$$

where τ denotes the transmissivity of the atmosphere from the sensor to any level, and τ_s the transmissivity to the background radiator with temperature T_s and emissivity e_s of the emitting surface. The first integral represents the contribution of the atmosphere and the second, that of the background. Although we may assume that $e_s=1$, the measured effective radiant emittance expressed by Eq. (2) is not a unique function of T_s due to the influence of the atmosphere which would change the first integral as well as τ_s in the second integral.

In accordance with the NASA definition we use the term equivalent blackbody temperature T_{BB} to designate the temperature obtained by equating Eqs. (1) and (2). Thus, we obtain T_{BB} simply by converting measured effective radiant emittance into the corresponding temperature by using the curve in Fig. 3 or Eq. (1).

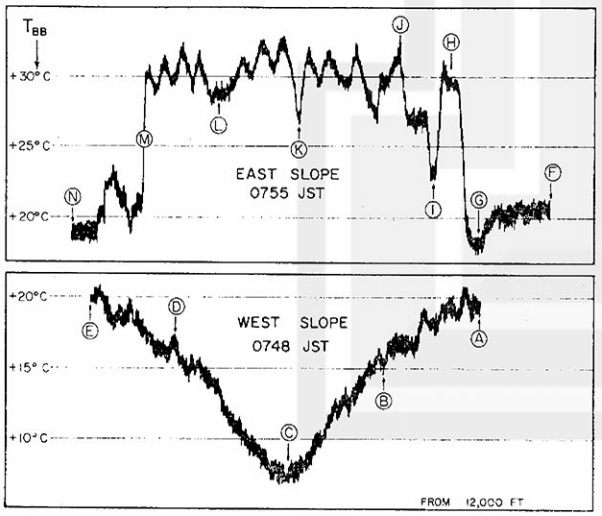

FIG. 5. Examples of recorded traces obtained on 28 July 1967 from the east slope (upper) and the west slope scanning. About 2 min were spent in completing a V-shaped scan. Horizontal lines represent the equivalent blackbody temperatures without corrections due to water vapor absorption.

3. Slope temperature of Mt. Fuji heated by the early morning sun

A circular flight at 12,000 ft around Mt. Fuji was made shortly after sunrise on 28 July 1967. A hand-held radiometer scanned along four separate scan lines shown in Fig. 4. Each scan was completed in about 2 min leaving an inverted V-shaped scan line. The topography of the mountain up to its height of 3776 m is shown with contour lines drawn for every 500 m. The areas of rocks and sand distribute asymmetrically down from the inactive crater at the top.

The recorded traces along two scan lines indicated by the letters A through E and F through N are reproduced in Fig. 5. The circled letters in Figs. 4 and 5 correspond

to each other. The traces show that the equivalent blackbody temperature decreased from A to C as the scan spot moved upward along the western slope which was still in the shadow of the mountain. The rise in temperature from C to E took place almost symmetrically to the scan-up trace.

Of particular interest is the temperature trace obtained while scanning along the eastern slope which had been in the sun since 0446 JST, the sunrise time. As expected, the equivalent blackbody temperature dropped a few degrees while the scan spot advanced from F to G. Upon reaching a small area of rocks at H the temperature jumped by 13C then plunged down while crossing a narrow grassland separating the small rocky area from the main area of rocks and sand. From J to M, the temperature went up and down keeping a mean value of about 30C regardless of the elevation of the slope.

The distribution of the equivalent blackbody temperature on the mountain slope is presented in Fig. 6 which also includes the direction and the elevation angles of the sun between sunrise and the time of the radiometric measurement. It will be found that the temperature decreases with height over the slope regardless of the sunlit and the shadow sides, except over the rocky and sandy slope illuminated by the morning sun. There are two hot spots on the east slope. The one near the mountain top was probably due to the lesser atmospheric absorption of shortwave radiation and to the large angle between the slope and the incoming ray. The other at a lower elevation would be due to the lapse rate of the ambient atmosphere which resulted in a higher mean temperature during the night.

Two days earlier, on 26 July 1967, a series of near-infrared pictures was taken looking south from Funatsu Weather Station. The meteorological conditions around the mountain were almost a carbon copy of those on the day of our experiment. The pictures in Fig. 7 show that the cumulus clouds on the east slope became thicker and thicker between 0845 and 0917 JST when the elevation angle of the sun increased from 47° to 53°.

It would be desirable to obtain detailed meteorological data along the eastern slope while airborne measurements are being made. Even though no such attempt was made at this time, it was learned that the Japan Meteorological Agency (1958) had operated several network stations along the slope. From these data we selected 18 August 1952, a day when meteorological conditions were very similar to those of 28 July 1967, for making the time sections of clouds, winds, surface, and air temperatures shown in Fig. 8. The locations of the stations numbered 1 through 5 appear in Fig. 4. All stations are approximately in line with the 110° azimuth from the highest station at 3775 m on the southwest rim of the crater. As seen in Fig. 8, the lowest station at 468 m was covered with stratus cloud during most of the night hours. Only scattered to broken cumuli were reported following sunrise. Station 2

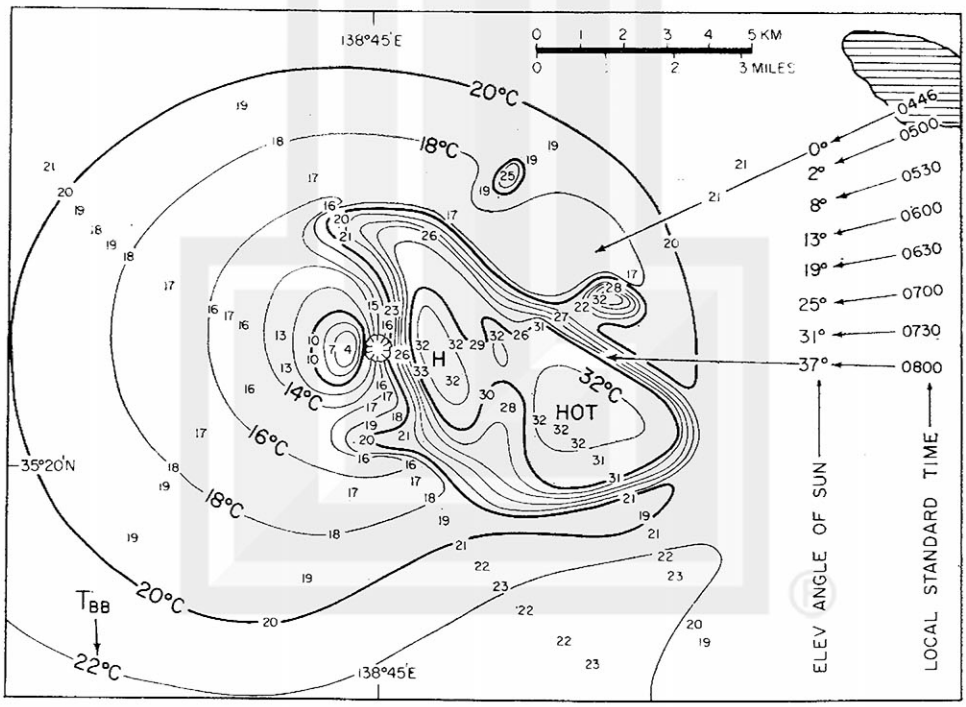

FIG. 6. Distribution of the equivalent blackbody temperature obtained by the PRT-4 radiometer between 0743 and 0756 JST 28 July 1967. The distance from the aircraft to the scan spots varies between 5 and 15 km, resulting in a variation of the scan-spot size between about 150 and 500 m in diameter. The azimuth and the elevation angle of the sun in the figure show that the east slope has been heated since 0500 JST.

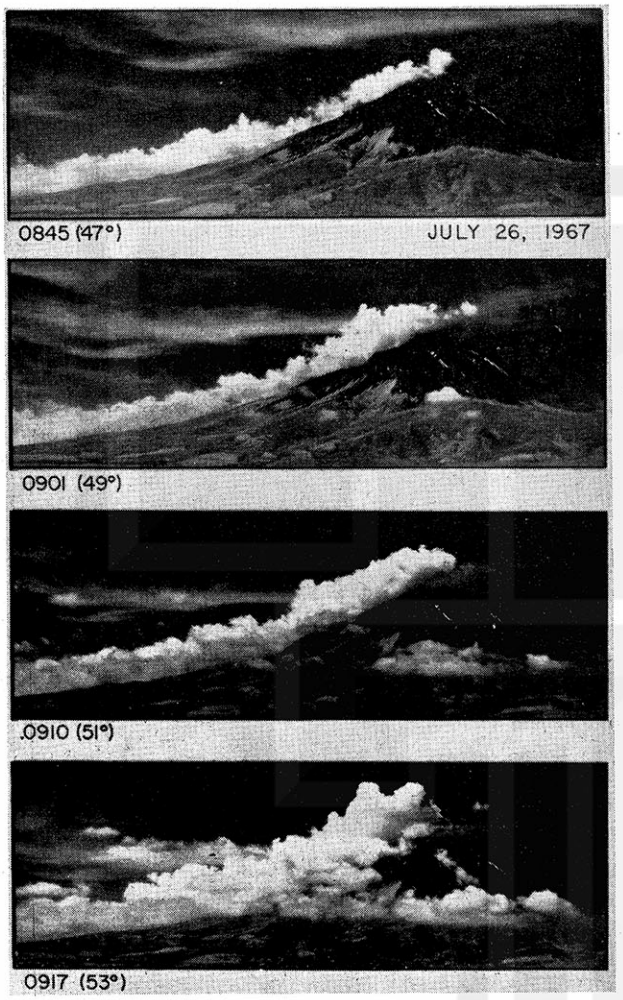

FIG. 7. Stages of the formation of cumulus clouds along the east slope of Mt. Fuji. Pictures were taken from Funatsu Weather Station on 26 July 1967, two days before the radiation measurements (courtesy of Saburo Yamamoto and Yadoru Yuyama).

at 1300 m, located in a wooded area, showed a gradual rise in the surface temperature. Due to the fact that the station was located just outside the rocks and sand area, it was in the cumulus base continuously between 0900 and 1800 JST. Stations 3, 4 and 5 located in the rocks and sand area showed a marked rise, as much as 30C, in the surface temperature. Cumulus formation took place over stations 3 (2780 m) and 4 (3240 m), suggesting that the patterns of cumulus along the slope would have been just like those presented in Fig. 7. It is of interest to find that the rise in the air temperature measured inside the instrument shelter was gradual, amounting to only a few degrees and showing no response to the abrupt rise in the surface temperature.

Results of our radiometric measurements, infrared photography from Funatsu station, and network station data collected during past years revealed that the rocky slope of Mt. Fuji is heated very rapidly by the early morning sun while the shady slope remains cool during early morning hours. A significant heat source along the east slope early in the morning stimulates the cumulus formation, thus providing a natural laboratory for studies of orographic convection involving solar heating effects. It was found that the equivalent blackbody temperature measured from an aircraft is very useful in learning the mode of heating and cooling of the mountain slope with various radiative characteristics ranging from those of a rocky and sandy slope to wooded ground at low levels.

4. Height and nadir-angle dependence of the equivalent blackbody temperature measured over land and water

Two areas for aerial measurements of radiation were selected in order to study the effects of the height and the nadir angle in determining the equivalent blackbody temperatures by means of indirect sensing from the air. The first area selected was over Sagami Bay (Fig. 9) with an approximate 26C sea-surface temperature. The area was relatively smog-free with surface visibility in excess of 20 km as shown in Fig. 1. The second area was selected over the western part of Tokyo covered with medium density smog reaching to 910 mb. A separate thin layer of smog was seen at about the 900-mb level (Fig. 10).

During the radiation measurements the aircraft flew at a constant pressure altitude while the hand-held radiometer was raised from a minimum nadir angle of about 40° to a maximum of 100°. The observer's hand was placed momentarily in front of the radiometer when the scan spot crossed the apparent horizon. The angular velocity of the sensor was kept more or less constant manually so that the nadir angle of view can be obtained by dividing the recorded trace at uniform intervals. During the measurement at each height between 500 and 10,000 ft, the sensor was raised upward to a 100° nadir angle followed by a return to the minimum nadir angle.

The equivalent blackbody temperatures obtained from altitudes of 1000, 2000, 4000, 6000, 8000 and 10,000 ft were plotted and contoured in Fig. 11. Both the pressure and the pressure altitude of the aircraft appear along the right and the left sides. The nadir angle increases toward the right from 0 to 120°.

The contour lines drawn for the T_{BB} show that the measured value increases to a maximum of more than 26C when the aircraft altitude increases to about 2000 ft, suggesting that the atmosphere below this level was warmer than the sea surface. By extrapolating the measured values down to the sea surface, the sea-surface temperature was estimated to be slightly less than 25C. After the completion of our radiometric measurements, it was learned that the sea-surface temperature beneath our flight path was about 26C according to direct measurements.

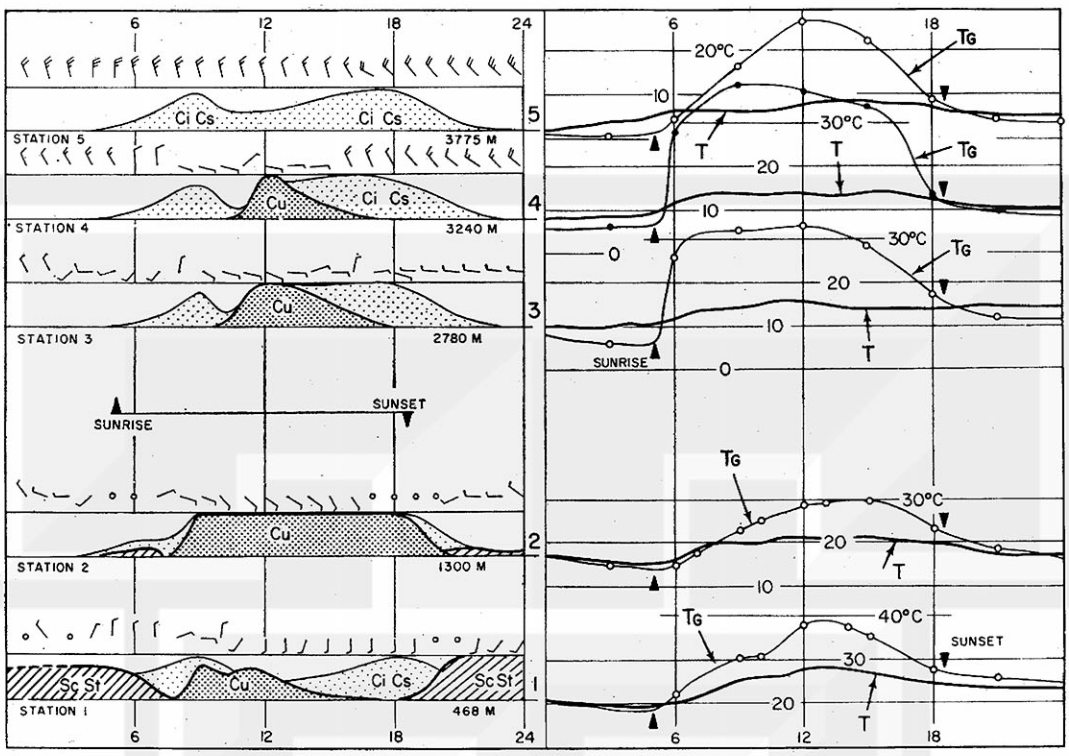

FIG. 8. Time cross sections of meteorological parameters observed at five stations along the east slope of Mt. Fuji. T_G denotes the ground temperature, T the air temperature measured inside the instrument shelter, and black triangles, the times of sunset and sunrise.

If we know the temperature and humidity distribution over the sea surface, it is feasible to compute the equivalent blackbody temperature as a function of pressure or pressure altitude and the nadir angle of view. Now we shall discuss the result of our computation made by using a 7094 computer at the University of Chicago.

In computing the radiance $N(\lambda,T)$ reaching the airborne detector by using the radiative transfer equation,

$$N(\lambda,T)=\int_{\tau_0}^{1}\frac{B(\lambda,T)}{\pi}d\tau+\frac{B(\lambda,T_s)}{\pi}\tau, \qquad (3)$$

and the spectral response ϕ_λ of the PRT-4 radiometer, we divided the spectral range between 7.4 and 16.0 μ

FIG. 9. The Sagami Bay area where the nadir angle and the height dependence of T_{BB} were obtained. Note that the east slope of Mt. Fuji is covered with scattered cumuli.

FIG. 10. The western part of Tokyo where radiation measurements were made by changing both nadir angles and flight levels. The city was covered with a light to moderate smog. The air above the smog top was very clean.

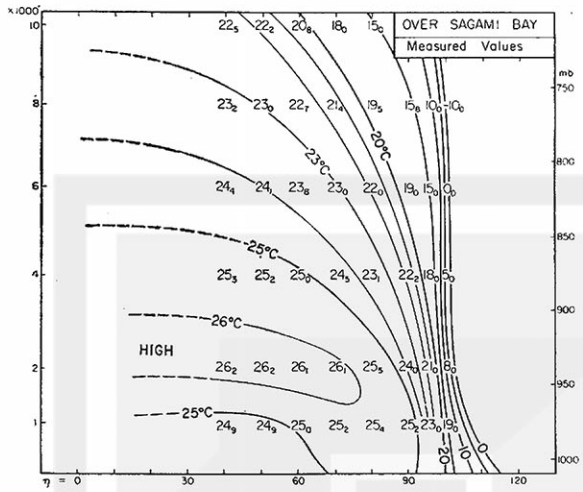

FIG. 11. Patterns of T_{BB} measured over Sagami Bay between 0811 and 0843 JST 28 July 1967. The sea-surface temperature is extrapolated to be about 24.5C.

(see Fig. 2) into 43 parts each with 0.2 μ intervals. Then the transmissivity between the aircraft and a specific layer, either above or below the aircraft, was computed by dividing the atmosphere into 40 layers of 20 mb each located between 1010 mb at sea level and 210 mb.

Then we computed the effective optical path u_e given by

$$u_e=\frac{\sec\eta}{g}\int_{P_a}^{P}\frac{P}{P_0}q\,dP, \tag{4}$$

where P_a is the static pressure at the flight level, $P_0=1000$ mb, q the mixing ratio and η the nadir angle of view. Absorption by CO_2 was not included.[2]

For the window region between 8.1 and 12.9 μ, we used the approach of Wark *et al.* (1962) in which the transmissivity for a specific wavenumber or wavelength is expressed as a function of u_e only. Outside the window region, we approximated the calculation by neglecting the temperature effect so as to use Elsasser's (1942) generalized absorption coefficient,

$$\tau=f(u_eL). \tag{5}$$

Because the spectral radiance on both sides of the window region will be reduced significantly by the spectral response of the PRT-4, we used the τ vs u_eL relationship at $P_0=1000$, used by Wark *et al.* in their computation.

Assuming the aircraft to be at the top of a layer for the convenience of computation, spectral transmissivities from the aircraft to either the bottom (when looking down) or the top (when looking up) of all 40 layers were calculated. After changing Eq. (3) into radiant emittance form,

$$W_\lambda=\int_{\tau_s}^{1}B(\lambda,T)d\tau+B(\lambda,T_s)\tau_s, \tag{6}$$

in order to obtain T_{BB} from Eq. (1), we write it in the difference form

$$W_\lambda=\sum_{n=1}^{n=a}B(\lambda,T_n)\Delta\tau_n+B(\lambda,T_s)\tau_s \tag{7}$$

for the looking-down case and

$$W_\lambda=\sum_{n=a+1}^{n=b}B(\lambda,T_n)\Delta\tau_n \tag{8}$$

for the looking-up case. The layer number $n=1$ is assigned to the bottom layer, $n=a$ to the layer just below the aircraft, and $n=b$, the uppermost layer.

The effective radiant emittances for the looking-down and the looking-up cases are written, respectively, as

$$\bar{W}=\sum_{m=1}^{m=c}\sum_{n=1}^{n=a}\phi_\lambda B(\lambda_m,T_n)\Delta\tau_n\Delta\lambda+\sum_{m=1}^{m=c}\phi_\lambda B(\lambda_m,T_s)\tau_s\Delta\lambda, \tag{9}$$

and

$$\bar{W}=\sum_{m=1}^{m=c}\sum_{n=a+1}^{n=b}\phi_\lambda B(\lambda_m,T_n)\Delta\tau_n\Delta\lambda, \tag{10}$$

where $\Delta\lambda=0.2\,\mu$ for this case. The effective radiant emittances computed from Eqs. (9) and (10) were converted into equivalent blackbody temperatures from Eq. (1) or Fig. 3.

A computed result appears in Fig. 12 in which T_{BB}

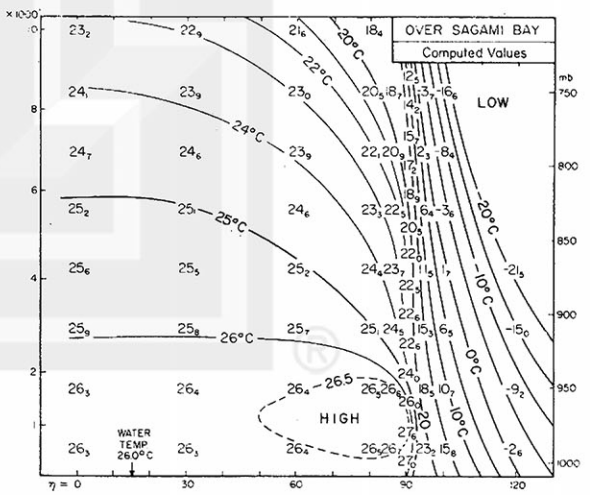

FIG. 12. Computed patterns of T_{BB}. The sea-surface temperature of 26.0C and the air temperatures entered along the vertical through $\eta=90°$ were used as input data.

[2] Due to the fact that the spectral response extends to 16 μ, the absorption by CO_2 will affect the measured values to a certain extent. However, the filtered energy within this absorption band is no more than 10% of the total effective radiant emittance. Estimates indicated that the error due to the CO_2 omission does not exceed 1–2C in measured temperatures.

was plotted and contoured at 5C intervals with heavy lines and at 1C intervals with light lines. The input air temperatures are seen along the vertical through the 90° nadir angle at which the radiometer measures the temperature at the flight level, because $\sec\eta$ in Eq. (4) reaches infinity. The maximum temperature, 27.6C at about 1000 ft above the 26.0C sea surface, results in an increase in T_{BB} of a few tenths of a degree when the aircraft altitude increases to about 1000 ft. Above this altitude T_{BB} decreases as the flight level increases.

Similar measurements were repeated over Tokyo on 28 July 1967. The city was covered with light to moderate smog reaching to about 910 mb (Fig. 10). A separate thin layer was seen at the 900-mb level which was approximately the base of convective clouds. A few pieces of very low stratus clouds were located at about the 960-mb level. In our radiation measurements none of these clouds were scanned to avoid undesirable consequences. Measurements started at the 10,000-ft pressure altitude where the air was clean with extremely high visibility permitting us to see distant mountains to the west and north. The measured equivalent blackbody temperature dropped sharply when the sensor axis was raised beyond the apparent horizon. The first indication of smog at the flight level was felt when the aircraft descended from 4000 to 2000 ft. At the time of the scan from the 2000-ft level it was noticed that T_{BB} did not decrease as it did at the higher levels when the radiometer was pointed a few degrees above the apparent horizon. The response to the space background was much slower when measured from the 1000-ft altitude, the lowest flight altitude permitted over Tokyo. The result of measurements over Tokyo appear in Fig. 13 in which the smog-covered portions in the diagram are stippled.

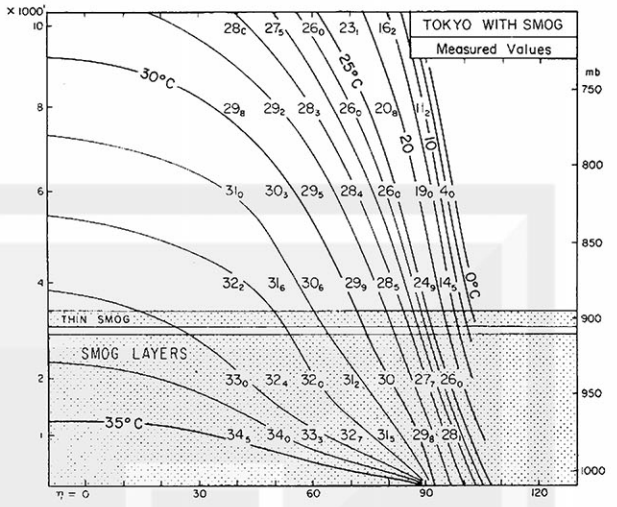

FIG. 13. Patterns of T_{BB} measured over Tokyo between 1115 and 1142 JST 28 July 1967. The levels of smog layers over the city are stippled.

In view of the existence of smog over Tokyo, efforts were made to compute equivalent blackbody temperatures taking the influence of smog into consideration. No satisfactory experimental data for such computations are available as far as Tokyo smog is concerned. Unlike the case of Los Angeles smog, residents rarely feel eye irritation in Tokyo although the smog reduces the visibility, resulting sometimes in a dim sun even at midday.

In our computation we assumed that the smog in question is a graybody within the spectral range of the PRT-4 radiometer. This assumption may not seem valid because the largest size of aerosols in the atmosphere is no larger than 10 μ. In their computation of visibility from the particle-size distribution, Pueschel and Noll (1967) showed, however, that the concentration of large-size aerosols is one order of magnitude larger in an urban atmosphere than in a maritime atmosphere. Barret and Ben-Dov's (1967) measurements by lidar also indicated that the concentration inside a plume reached 3 mg m^{-3} in a 200-ft thick layer, showing that it was about two orders of magnitude larger than normal conditions. If Tokyo smog contains considerable numbers of particles in excess of 10–20 μ, our assumption of gray smog may not be too far from realistic.

We make the further assumption that the transmissivity inside the smog decreases exponentially as

$$\tau^* = e^{-k\Delta P\sec\eta}, \tag{11}$$

where τ^* denotes the transmissivity in the direction of nadir angle η and ΔP is the pressure difference at the top and the bottom of the smog which attenuates the radiant energy. Then we define the smog according to its absorptivity α^* when radiation penetrates vertically through a 100-mb depth, i.e.,

$$(1-\alpha^*) = \tau^* = e^{-100k}, \tag{12}$$

where k should be expressed in mb^{-1} units. If we designate graybody smog as No. 1, 2, 3, $\cdots$, 9, corresponding, respectively, to absorptivities $\alpha^* = 0.1, 0.2, 0.3, \cdots, 0.9$, the the corresponding values of k are 1.06, 2.23, 6.93, $\cdots$, 16.09 in 10^{-3} mb^{-1} units. A blackbody smog or No. 10 smog is therefore characterized by $\alpha^* = 1.0$ or $k =$ infinity.

In order to find out the influence of smog upon T_{BB} measured from various altitudes, T_{BB} was computed for the cases of no smog, and for smog Nos. 2, 5 and 8. The results in Fig. 14 reveal that T_{BB} decreases rather rapidly as the aircraft height inside the smog increases. The rate of decrease, as expected, becomes pronounced as the smog number increases. In the case of a blackbody smog, T_{BB} and the smog temperature should coincide.

Of importance is the contribution to the radiation from the ground upon the effective radiant emittance measured at the various aircraft altitudes. We define

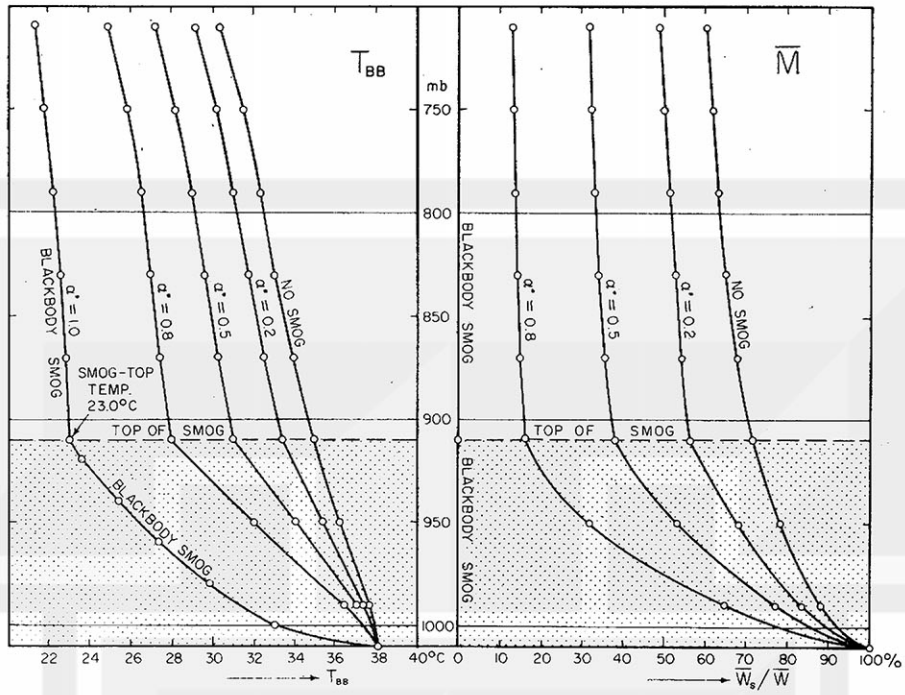

FIG. 14. Decrease in T_{BB} measured downward from various altitudes scaled in mb (left). The density of smog was changed from transparent to blackbody smog. Mixing ratio of surface radiation $\bar{M}$ also decreases as the flight level increases. Note that the blackbody smog gives $\bar{M}=0$ at all altitudes.

the ratio

$$\bar{M}(h,\eta)=\frac{\bar{W}_s(h,\eta)}{\bar{W}}, \tag{13}$$

where $\bar{W}_s(h,\eta)$ denotes the effective radiant emittance of the surface reaching the airborne radiometer after passing through the atmosphere including moisture and smog, $\bar{W}$ the total effective radiant emittance, and $\bar{M}(h,\eta)$ the ratio which may be called the "mixing ratio of surface radiation." It should be noted that the surface temperature can be related uniquely to the measured $\bar{W}$ only if $\bar{M}=1$.

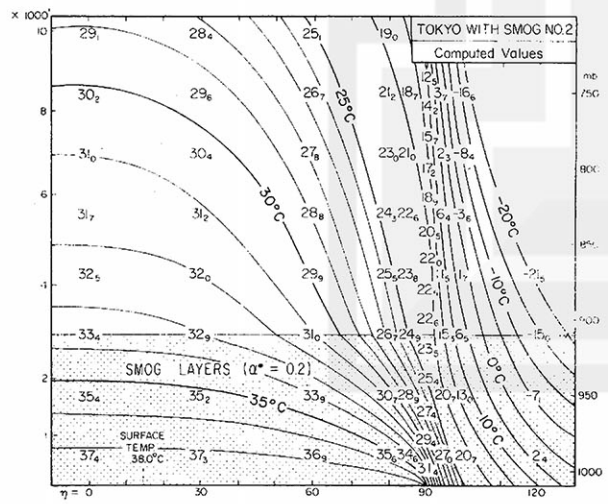

FIG. 15. The best fit patterns of T_{BB} over Tokyo obtained by introducing a smog of 0.2 absorptivity when looking down through a 100-mb atmosphere.

The right-side diagram in Fig. 14 shows the decrease in the relative contribution of the ground as the height and the smog number increases. Due to the radiation from water vapor below the flight level, $\bar{M}$ decreases to about 60% when measured from 700 mb without smog. If smog behaves as a blackbody, $\bar{M}$ will be zero at all altitudes, indicating that we are not able to determine the radiative characteristics of the ground from aerial measurements.

It would be difficult to obtain the radiative characteristics of the smog over Tokyo when our radiation measurements were made on 28 July 1967. However, the pattern of T_{BB} in Fig. 13 may reveal the smog conditions under discussion. An attempt was made, therefore, to obtain a large number of computed T_{BB} patterns by changing both the smog numbers and the surface temperatures. A combination of 1 through 9 smog numbers and the surface temperatures 34 through 44C at 2C intervals was studied carefully, leading to the conclusion that the surface temperature of 38C combined with No. 2 smog ($\alpha^*=0.2$) gives the closest pattern to that of the measured one.

The best-fit pattern thus obtained is presented in Fig. 15. The figure shows that the layer of smog No. 2 attenuates the radiation from the ground, resulting in

a 4.6C reduction when measured vertically from the smog top. The corresponding reduction without smog is computed to be 3.0C. The lapse rate of T_{BB} above the smog layer is relatively small, only about 0.6C $(1000\,\text{ft})^{-1}$.

5. Damping factor and crossover temperature

Due to the fact that the effective radiant emittance reaching a radiation sensor always includes the atmospheric radiation, the equivalent blackbody temperature corresponding to the measured $\bar{W}$ differs from the surface temperature. By computing a large number of model atmospheres, Wark *et al.* (1962) showed a statistical result that the satellite-measured T_{BB} from the 8–13 μ channel is almost always lower than the surface temperature. Our results obtained from airborne measurements also show a significant reduction in the measured T_{BB} as the height increases, except near the altitude of temperature inversion.

Since the difference between T_{BB} and the surface temperature is a result of the fractional contribution of the atmospheric radiation to the total effective radiant emittance, the atmosphere will also reduce the variation in the surface temperature. In other words, the variation, both in time and space, in the surface temperature measured through the atmosphere decreases as the aircraft altitude increases.

We shall now define the damping factor D as

$$D=\frac{\Delta T_{BB}}{\Delta T_s},$$

where T_{BB} denotes the measured value, T_s the surface temperature, and Δ their variation. The surface may be the ground, the sea surface, etc., as long as it emits as a blackbody.

In order to determine the damping factor over Sagami Bay, the sea-surface temperature was changed from 20 to 30C at 2C intervals while keeping the overlaying atmosphere unchanged. In reality, however, the low-level atmosphere would be modified due to air-sea interaction. Nevertheless, such a condition could exist where a uniform air mass stays over the sea surface characterized by a tight temperature gradient or by areas of local hot and cold spots. Fig. 16 shows the variations of T_{BB} thus computed. The input air temperatures and mixing ratios appear to the left at 20-mb intervals. The figure reveals that the damping factor, 77% at 500 m, decreases to 51% as the height increases to beyond 5 km. From the satellite level, a damping factor of 50% should be assumed in this case if this instrument were to be used.

In view of such low values in the damping factor, it is necessary to correct the measured ΔT_{BB} over a small region in order to obtain the thermal gradient over the

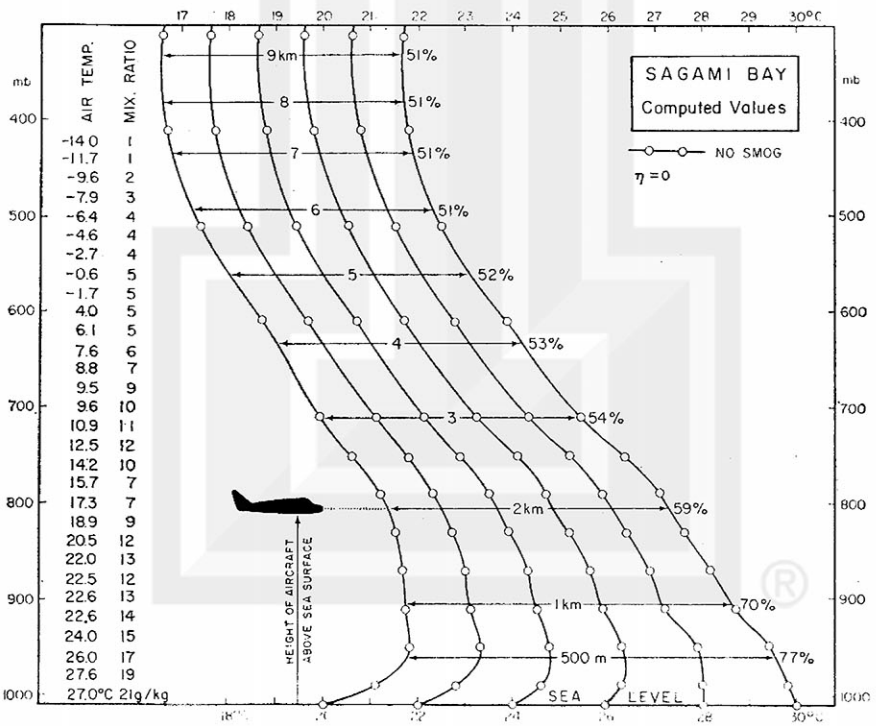

FIG. 16. Change in T_{BB} of six targets measured from various altitudes up to 10 km. The temperature and the mixing ratio of the atmosphere were kept unchanged while the target temperatures were increased from 20 to 30C at 2C intervals.

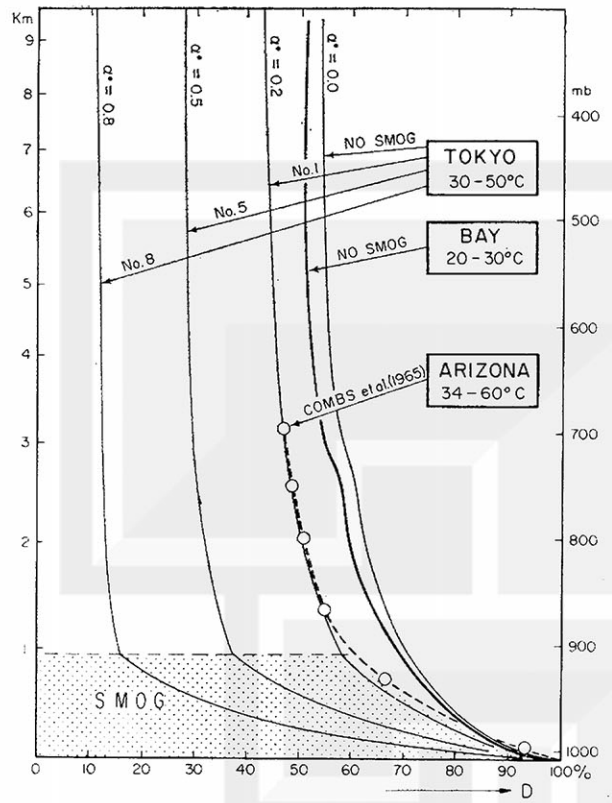

FIG. 17. Decrease in the temperature damping factor D as a function of the aircraft height above the radiating surface. The values were computed at zero nadir angle. One case without smog and three cases of varying smog over Tokyo indicate that smog damps the surface temperature variations measured by an airborne radiometer.

sea surface. This fact necessitates a large correction unless an aircraft flies less than 100 ft above the surface for which the damping factor would be about 90%. For a high-level flight necessary to achieve a large-area scan, we must know the thermal characteristics of the atmosphere below the flight level so as to perform required corrections afterward.

The damping factor over Tokyo was computed under various smog conditions by increasing the aircraft altitude up to 10 km. The result in Fig. 17 shows the obvious effects of smog, which increase with the absorptivity α^*. The damping factor of 0.64 applicable to the case without smog is reduced to 0.28 for smog No. 5 and further to 0.11 for smog No. 8, suggesting that only about 10% of the temperature variation at the surface will be measured from the 10-km level when the city is covered with a dense smog. Included also in the figure is the damping factor over the bay and over Arizona computed from the results by Combs *et al.* (1965). There are no simple ways of estimating the damping factor as a function of the height and the nadir angle unless the radiative transfer equation is solved numerically, taking into consideration the temperature and the humidity distribution inside the atmosphere as well as the temperature of the surface and smog conditions.

In order to convert the equivalent blackbody temperature T_{BB} measured from an aircraft into a corresponding surface temperature T_s, we rewrite Eq. (14) as

$$D=\frac{T_{BB}-T_{CO}}{T_s-T_{CO}}$$

or

$$T_s=T_{CO}+(T_{BB}-T_{CO})D^{-1}, \qquad (15)$$

where T_{CO} is a specific temperature satisfying the condition that $T_s=T_{BB}=T_{CO}$ when measured from a given aircraft height and nadir angle. The temperature T_{CO} may be called the "crossover temperature."

Fig. 18 was prepared for further explanation of the crossover temperature. The figure shows that computed values of T_{BB} for various surface temperatures measured through a specific atmosphere from $h_a=3000$ ft with a nadir angle of $\eta=0$ increase with T_s. The mode of increase in T_{BB} is more or less linear, crossing the straight line of T_s at a point indicated by a black circle at which T_{BB} and T_s are equal. The circle denotes the crossover point of two lines and the temperature at the circle is the crossover temperature. The tangent of the T_{BB} line obviously represents the damping factor D which can be measured on the diagram. Rigorously, of course, the damping factor D as defined by Eq. (14) is not necessarily a constant. This is reflected in the slight curvature of the T_{BB} line in Fig. 18.

It is important to note that both T_{CO} and D under given atmospheric and smog conditions are, respectively, a function of both aircraft height h_a and the nadir angle of view η. Thus, the surface temperature from Eq. (15) can be computed for given vertical distributions of temperature, water vapor, and smog or other assumed graybody matter after expressing T_{CO} and D as functions of h_a and η.

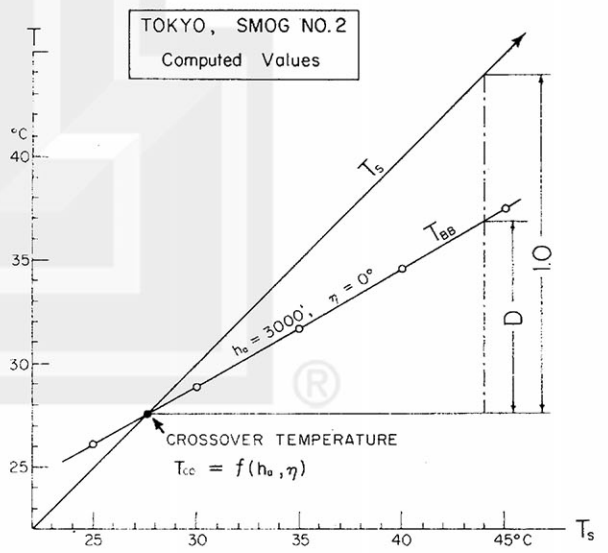

FIG. 18. A diagram for computing the crossover temperature T_{CO} and the damping factor D from computed values of T_{BB}. Tokyo with smog No. 2 was used for the computation while changing the surface temperature from 25 to 45C at 5C intervals.

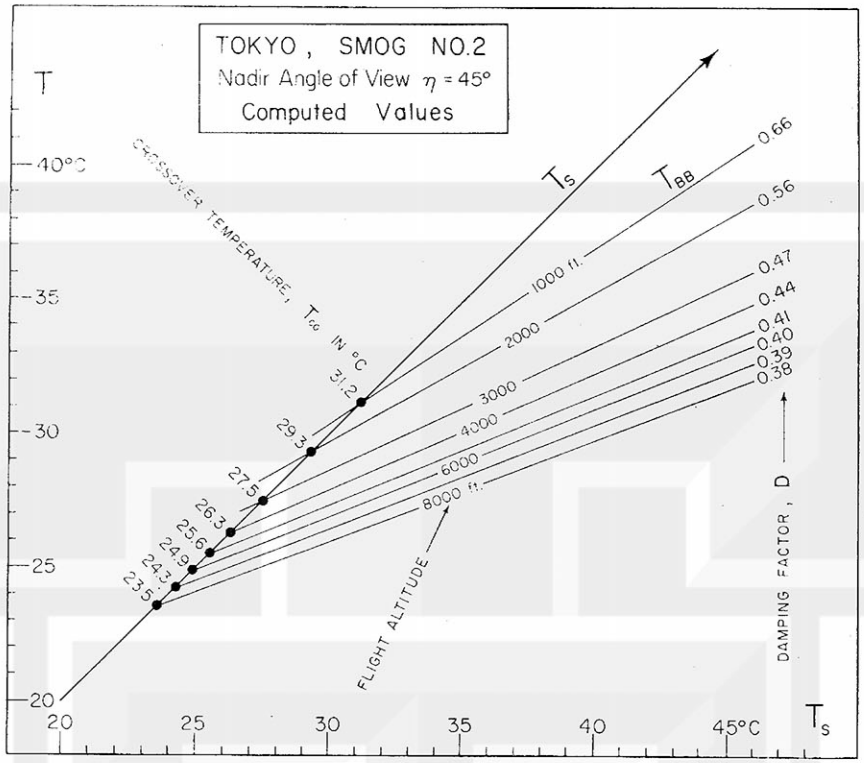

FIG. 19. Crossover temperatures and damping factors computed for a 45° nadir angle of view from aircraft altitudes between 1000 and 8000 ft. These values were used in estimating surface temperatures from equivalent blackbody temperatures measured over Tokyo on 28 July 1967.

6. Examples of temperature measurements over the Tokyo area

About ten temperature measurement locations were selected in an attempt to determine surface temperatures. Due to the fact that the variation of surface temperature is far more dramatic than that of air temperature, we selected several scan spots inside each predetermined location.

Although only three aircraft altitudes, 1000, 2000, and 3000 ft, were used in our experiment, equivalent blackbody temperatures were computed for altitudes at 1000 ft intervals up to 8000 ft. The nadir angle of view was kept at 45° since this angle was found to be most convenient in aiming a hand-held PRT-4 radiometer. Shown in Fig. 19 are the crossover temperatures and the damping factor for each altitude. It will be found that the variations in T_{BB} when measured from about 2500 ft should practically be doubled when converted into T_s. We are, of course, assuming that the atmospheric stratification over the Tokyo area is uniform. This assumption might not be true. As long as the radiative property of the atmosphere is concerned, however, expected irregularities are negligible in comparison with much greater variation in the radiant emittance of surfaces radiating under the midsummer sun.

Figs. 20 and 21 show six locations of T_{BB} measurements and recorded traces scaled in both T_{BB} and T_s. The latter was computed from Eq. (15) by using the values of T_{CO} and D in Fig. 19.

Ginza Avenue was scanned from 1000 ft, first looking west pointing toward the sides of buildings heated by the morning sun, then looking east toward the sides which had started to receive the afternoon sunlight. Due partially to choppiness caused by a low-altitude flight and also to the large structures on Ginza, no clear-cut temperature patterns were obtained. It may be stated, however, that the avenue in the shade shows a cool 34C while some building tops are quite hot, say 44C.

At the Japan Meteorological Agency (JMA), temperatures of asphalt and soil surfaces were measured at 1-hr intervals during the flight which started shortly before sunrise and ended in midafternoon. The variations in surface and air temperatures as well as those of wind and clouds are presented in Fig. 22. At 1025 JST when measured surface and air temperatures were about 41–45C and 31C, respectively, the shady side of JMA was 37C (T_{BB}=34C) and the sunlit side, 42C (T_{BB}=36C). Then the radiometer was pointed toward the Imperial Moat with shallow water to obtain 32C (T_{BB}=30C). These temperatures seem to be quite reasonable when compared with the ground measurements. It should be pointed out that the measured T_{BB} are far from actual T_s, thus necessitating proper corrections in order to calculate T_s from T_{BB} obtained indirectly from aircraft.

Meiji Shrine is surrounded by woods with trees 70–

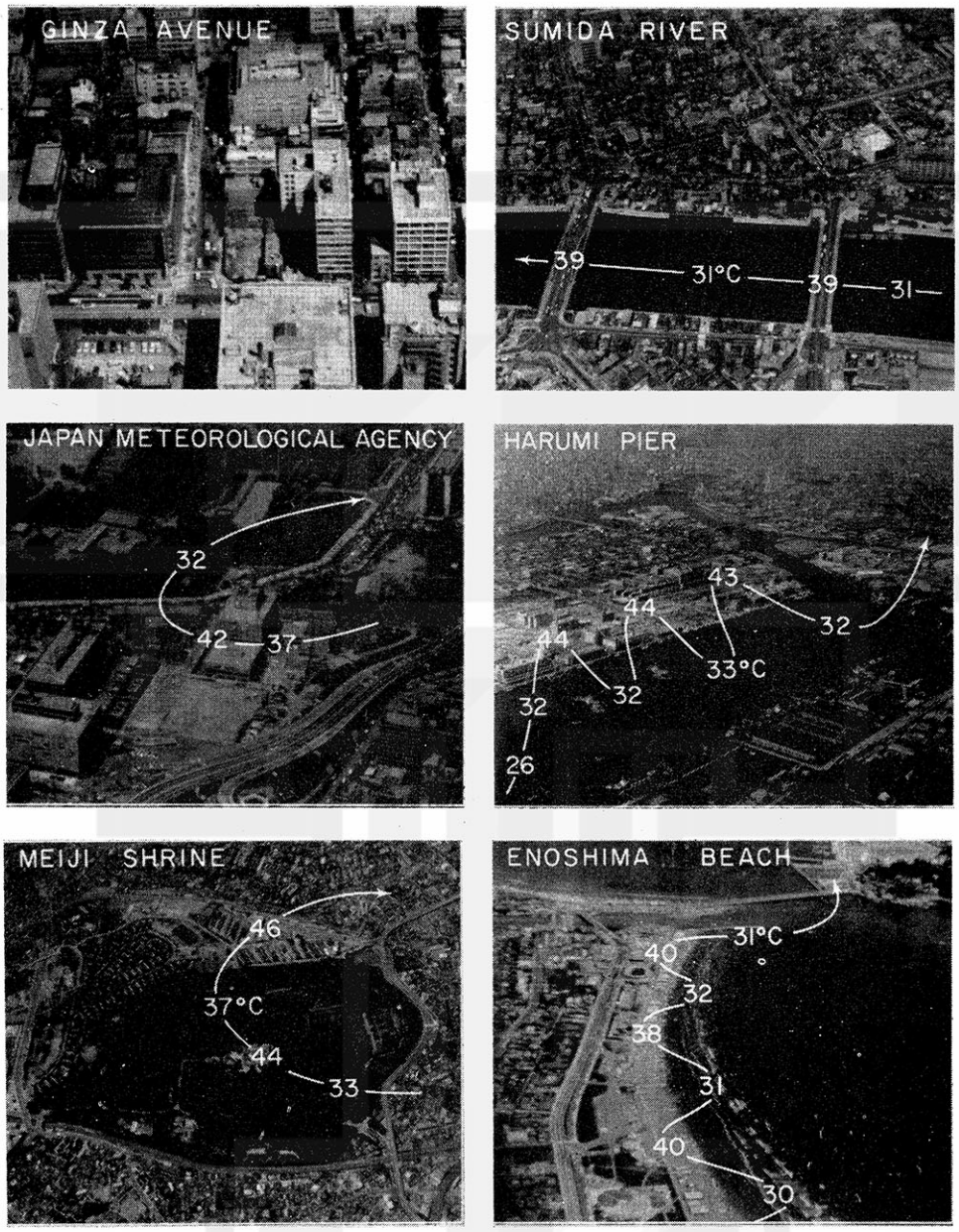

FIG. 20. Scan lines and surface temperatures superimposed upon aerial pictures taken on 28 July 1967, the day of radiation measurements. Pictures are Ginza Avenue looking east, Japan Meteorological Agency and a portion of the Imperial Moats, Meiji Shrine surrounded by extensive woods, Sumida River with Komagata and Azuma Bridges near Asakusa, Harumi Pier and Sumida River, and Enoshima beach.

130 years old. An arc-shaped scan with a short pause when pointing toward the shrine building, made at 1330, resulted in 33–37C tree-top temperatures. A 44C temperature of the building, with copper roofs renewed in 1958, seems to be several degrees lower than expected. It is very likely that the half-power scan spot, an ellipse of 100×150 ft, was too large to be kept on the roofs during a short measurement pause. Moreover, the full-power scan spot is expected to be several times larger than the integrated areas of the copper roofs. When the scan spot moved out into a residential area just outside the shrine, the estimated surface temperature increased to 46C with a peak maximum reaching 48C.

The Sumida River and several bridges were scanned with a short pause at each bridge crossing. The scan spot was placed in the river north of Azuma Bridge, resulting in a 31C water temperature. Two 39C peaks were recorded while crossing Azuma and Komagata Bridges. The third bridge showed a 37C temperature followed by a 30C water temperature. When the scan spot was moved to the river bank, T_s increased to 43C.

Harumi Pier with warehouses on the waterfront was scanned from 3000 ft in such a manner that the scan

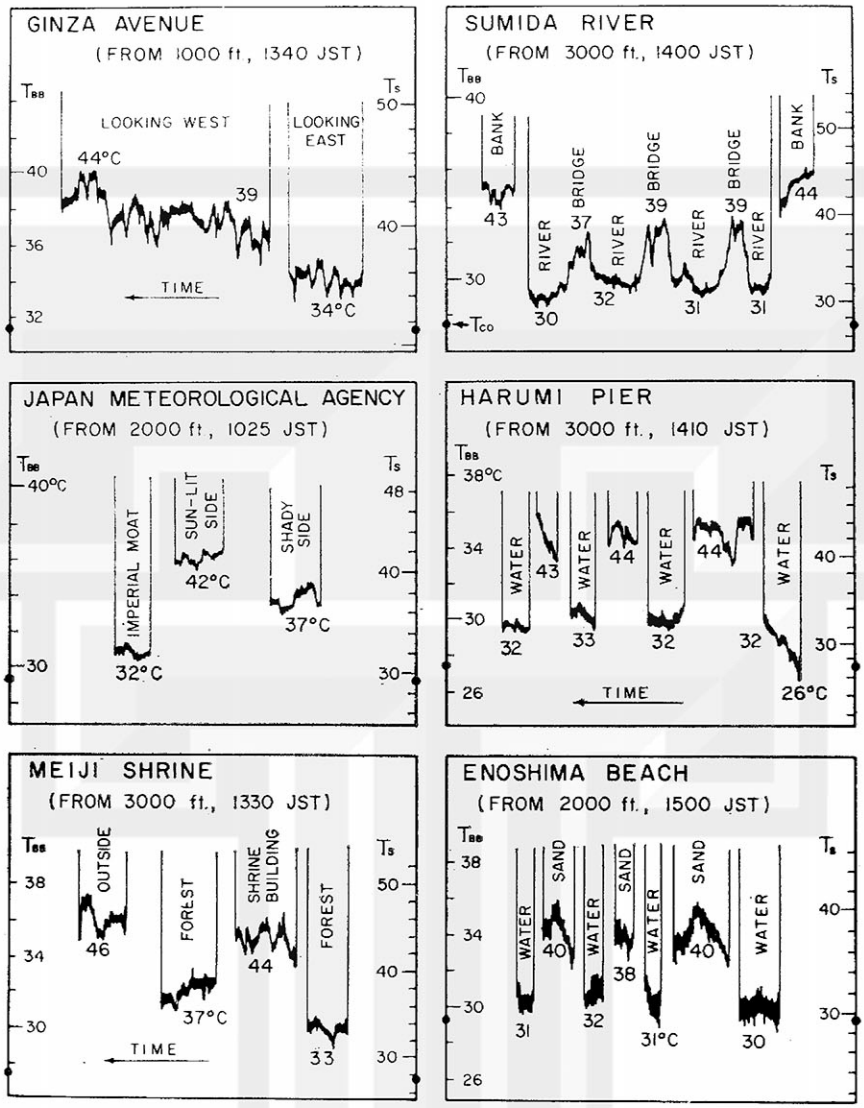

FIG. 21. Recorded traces obtained from six locations in the previous figure. The radiometer's field of view was obstructed by the observer's hand when the scan spot was moved from one object to the next. The temperature scale to the left indicates T_{BB} while the other one to the right is the surface temperature T_s computed from Eq. (10) and values of T_{CO} and D in Fig. 19.

spot was moved alternately from the water to the land. A temperature difference of about 12C was obtained. The lowest water temperature of 26C appeared at the time when the overwater scan started.

Enoshima Beach, crowded with people, was scanned at 1500 JST, the hottest time of the day. The spot was moved off-shore until the entire full-power scan spot moved into the water with breaking waves, then it was brought back to the sandy beach. Such a motion of the scan spot resulted in an average 31C water temperature and 40C sand-beach temperature. We expected to obtain much higher surface temperatures from the beach where one would feel much higher temperatures while walking barefoot.

These examples of surface temperatures estimated from airborne measurements of T_{BB} indicate that it is feasible to determine surface temperature efficiently. The estimated values show good agreement with those measured on the ground and also with those expected on a midsummer day.

7. Conclusions

The experimental results of airborne infrared measurements over the slope of Mt. Fuji, Sagami Bay and Tokyo revealed that a 8–13 μ radiometer is capable of measuring equivalent blackbody temperatures from various surfaces radiating at different temperatures. Due to atmospheric absorption and concurrent re-radiation, however, the measured equivalent blackbody temperatures are far from the temperatures of the radiating surfaces which may be assumed to be blackbody radiators for most practical purposes.

Since the amount of temperature correction applied to the equivalent blackbody temperature is a function

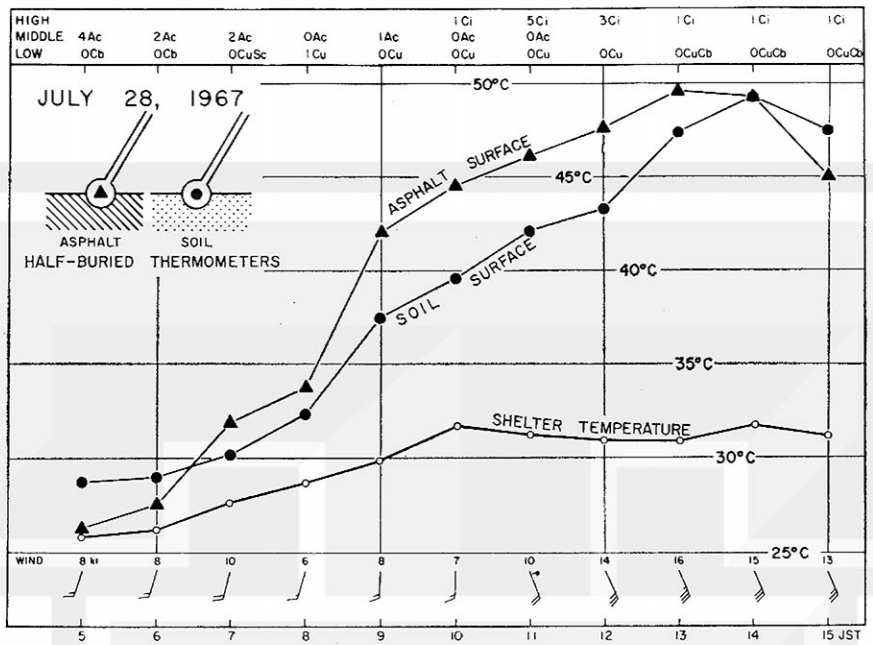

FIG. 22. Change in the surface and the air temperature at the Japan Meteorological Agency located near the northeast corner of the Imperial Palace. Note that surface temperatures reached almost 50C while air temperatures measured in the instrument shelter were only up to 32C. Shown at the top are types and amounts of clouds.

of the surface temperature to be estimated, it is necessary to obtain two parameters introduced in this paper. These are D, the damping factor, and T_{CO}, the cross-over temperature. Using these parameters, we are able to determine surface temperatures within an area over which the radiative properties of the atmosphere may be assumed uniform.

Measurement examples are given together with a correction method which will increase the accuracy of estimating the surface temperatures through indirect sensing of the effective radiant emittance in the 8–13 μ region.

A next logical step in further verification of these results is to apply them to problems such as the determination of sea-surface temperature from satellite and airborne radiometers, mapping of hot and cold spots over a vast heated plane, determination of water pollution by mapping the midday surface temperatures, etc. It will even be possible to determine the degree of air pollution if we measure the equivalent blackbody temperature of a surface of known temperature.

As a result of this study, it is recommended that radiometers, with cleaner window regions, such as the ones on board Nimbus satellites, be developed and tested for use in airborne radiometric measurements.

Acknowledgments. The authors are very grateful to the Asahi Newspaper for giving us ample flight time for the completion of our measurements. Acknowledgments are also due to Mr. Koichi Simizu of Asahi Sansho, who made a successful inflight recording of the radiation data used in this research and to Dr. Atsushi Kurashima for his kind efforts to initiate and carry out this experiment.

REFERENCES

Barrett, E. W., and O. Ben-Dov, 1967: Application of the lidar to air pollution measurements. *J. Appl. Meteor.*, **6**, 500–515.

Combs, A. C., H. K. Weickman, C. Mader and A. Tebo, 1965: Application of infrared radiometers to meteorology. *J. Appl. Meteor.*, **4**, 253–262.

Elsasser, W. M., 1942: Heat transfer by infrared radiation in the atmosphere. *Harvard Meteor. Studies*, No. 6, 101 pp.

Greenfield, S. M., and W. W. Kellogg, 1960: Calculations of atmospheric infrared radiations as seen from a meteorological satellite. *J. Meteor.*, **17**, 283–290.

Japan Meteorological Agency, 1958: Fuji-san no kisho (Weather at the summit of Mt. Fuji). Special volume giving the results of observations along the mountain slope, 79 pp.

Kuhn, P. M., and J. D. McFadden, 1967: Atmospheric water vapor profiles derived from remote-sensing radiometer measurements. *Mon. Wea. Rev.*, **95**, 565–569.

Lenschow, D. H., and J. A. Dutton, 1964: Surface temperature variations measured from an airplane over several surface types. *J. Appl. Meteor.*, **3**, 65–69.

Lorenz, D., 1966: The effect of the long-wave reflectivity of natural surfaces on surface temperature measurements using radiometers. *J. Appl. Meteor.*, **5**, 421–430.

——, 1967: Temperaturmessungen von Boden- und Wasseroberflächen von Luftfahrzeugen aus. *Geofis. Pura Appl.*, **67**, 197–220.

NASA, 1961: TIROS II radiation data users' manual. Goddard Space Flight Center, Greenbelt, Md.,

Pueschel, R. F., and K. E. Noll, 1967: Visibility and aerosol size frequency distribution. *J. Appl. Meteor.*, **6**, 1045–1052.

Wark, D. Q., G. Yamamoto and J. H. Lienesch, 1962: Methods of estimating infrared flux and surface temperature from meteorological satellites. *J. Atmos. Sci.*, **19**, 369–384.

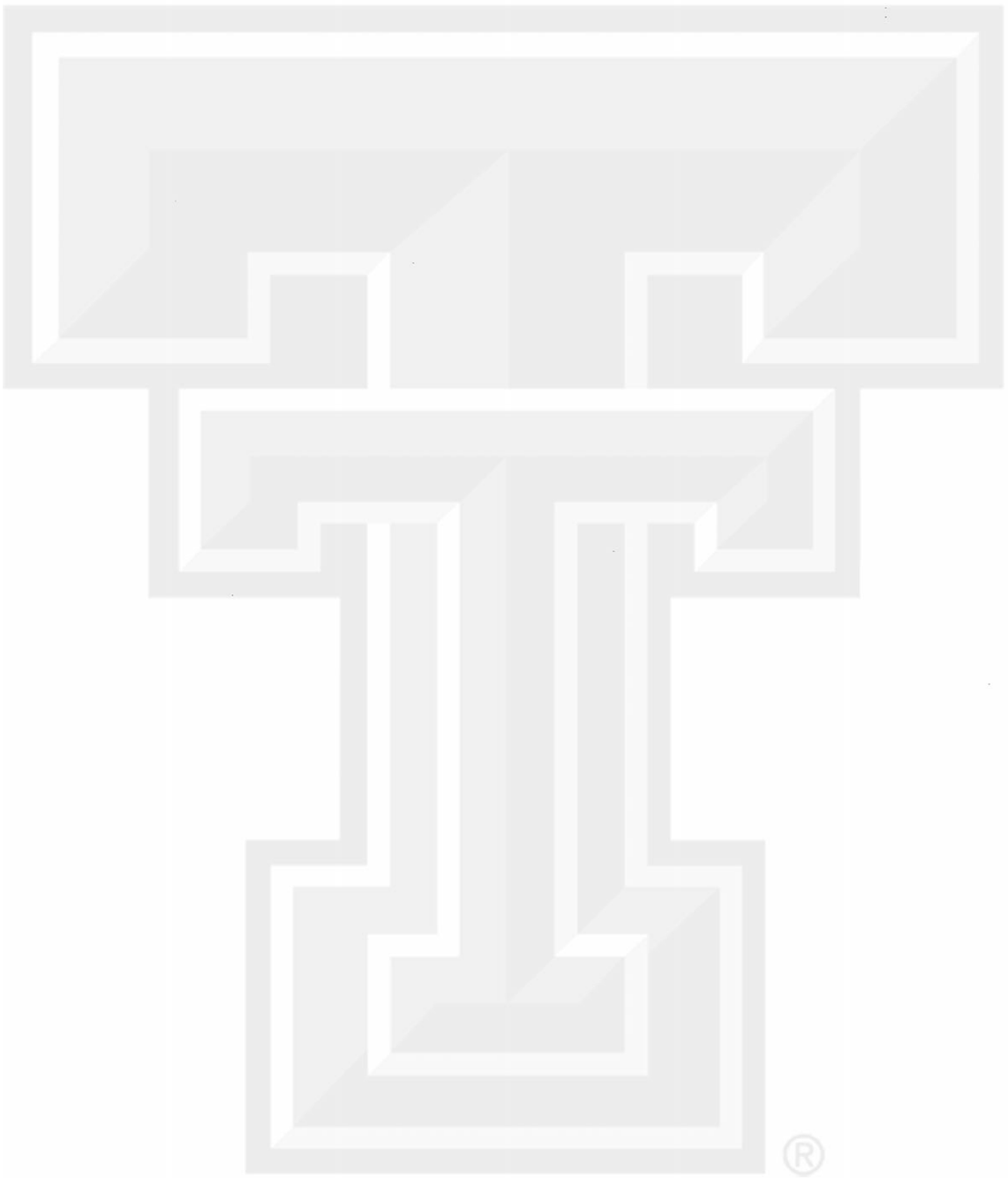

LANCASTER PRESS, INC., LANCASTER, PA.